Marine Geology 429 (2020) 106315

Contents lists available at ScienceDirect

Marine Geology

journal homepage: www.elsevier.com/locate/margo

Evaluating the effects of regional climate trends along the West Antarctic Peninsula shelf based on the seabed distribution of naturally occurring radioisotopic tracers

Richard S. Taylor[a,*], David J. DeMaster[a], Craig R. Smith[b], Carrie J. Thomas[a]

[a] Department of Marine, Earth and Atmospheric Sciences, North Carolina State University, Raleigh, NC 27695-8208, USA
[b] Department of Oceanography, University of Hawaii at Manoa, Honolulu, HI 96822, USA

ARTICLE INFO

Keywords:
Radiochemical flux
Seabed
Sea-ice
Climate change
Antarctica

ABSTRACT

Measurements of ^{230}Th, ^{14}C, ^{210}Pb and ^{234}Th activities were made on sediment cores collected along a N-S transect exhibiting a gradient in annual sea-ice duration off the West Antarctic Peninsula. The resultant data were used to evaluate the effects of regional warming on particle flux reaching the seabed on timescales from millennial to seasonal. Shelf samples were collected at five stations, over three cruises, between February 2008 and March 2009, as part of the FOODBANCS2 Project. Sea-ice conditions (the number of days ice-free prior to core collection) were evaluated at the five stations to understand the relationship between ice abundance and particle/radionuclide flux. Based on the millennial tracer ^{14}C, rates of sediment accumulation along the peninsula decrease southward, consistent with the observed sea-ice gradient. ^{230}Th data provide additional evidence on millennial timescales that sediment focusing (i.e., lateral transport) occurs to a greater extent in the northern reaches of the study area compared to the southernmost stations. The distribution of steady-state, ^{210}Pb flux to the seabed (representing centurial trends) displays a similar trend to ^{14}C, showing higher radionuclide/particle flux in the northern study area (where sea-ice duration is diminished) and lower flux southward as sea-ice duration increases. Additionally, ^{210}Pb data suggest that lateral transport plays an important role in the sediment distributions of this radiotracer on hundred-year timescales, which is explainable by the relatively short circulation times of peninsular waters relative to ^{210}Pb's half-life. On seasonal and annual time scales, the distribution of steady-state ^{234}Th flux to the seabed shows an increase in radionuclide flux at the southernmost stations. This increase in radionuclide flux on seasonal and annual time scales is consistent with the warming trend along the peninsula and the reduction in sea-ice duration over the past decade. A significant statistical relationship, however, could not be established between annual sea-ice free days and ^{234}Th-derived particle flux to the seabed. The fluxes/distributions of long-lived particle-reactive tracers (^{14}C, ^{230}Th, and ^{210}Pb) on the West Antarctic Peninsula shelf appear to be controlled primarily by the long-term pattern of increasing annual sea-ice duration in the southward direction, whereas the fluxes of the short-lived tracer (^{234}Th) are consistent with the more recent decreases in sea-ice duration (associated with climate change) that have occurred over the past decade, primarily in the southern West Antarctic Peninsula stations.

1. Introduction

Global warming is a non-local phenomenon that is impacting nearly every part of the planet. However, not all regions are impacted equally. High-latitude, polar-regions are experiencing some of the greatest increases in air and water temperatures (Meredith and King, 2005; Mulvaney et al., 2012). Reported air temperatures during the West Antarctic Peninsula (WAP) winters have warmed over 5 °C since 1950 (Mayewksi et al., 2009; Turner et al., 2013), and the annually averaged air temperature has risen ~3 °C (Meredith and King, 2005; McClintock et al., 2008). Although there has been a period of cooling along the WAP from 1997 to 2014 (Turner et al., 2016), the cooling up to 2009 (the time of this study) has been small compared to the warming documented from 1950.

As a consequence of global heat retention, westerly wind intensity has increased around Antarctica (Mayewksi et al., 2009; Fan et al., 2014), reducing annual sea-ice extent along the WAP, i.e., producing decreased sea-ice duration per year (Harangozo, 2006; Stammerjohn

* Corresponding author.
E-mail address: rtaylor@ncsu.edu (R.S. Taylor).

https://doi.org/10.1016/j.margeo.2020.106315
Received 19 April 2019; Received in revised form 20 July 2020; Accepted 3 August 2020
Available online 11 August 2020

et al., 2008; Smith et al., 2012). On the WAP, the increased air temperature has translated into a 1 ˚C increase in the surface ocean temperature along the peninsula (Meredith and King, 2005; Turner et al., 2014). Increased sea-surface temperatures have been shown to be a contributing factor in the decrease of sea-ice on the WAP (Jacobs and Comiso, 1993; Stammerjohn et al., 2008; Fan et al., 2014). Sea-ice extent has diminished along the WAP by 40% since satellite measurements began in 1978, and there has been a 90-day decrease in average sea-ice days (over the last 30 years) within the Palmer LTER area (Stammerjohn et al., 2008; Ducklow et al., 2013).

The WAP exhibits a wide ranging and complex ecosystem, and much of the marine ecosystem dynamics are coupled to seasonal sea-ice parameters, e.g., the timing of sea-ice advance/retreat (McClintock et al., 2008; Montes-Hugo et al., 2009; Ducklow et al., 2012; Smith et al., 2012; Rozema et al., 2016). As a result, many pelagic species have evolved to have life cycles synchronized with sea-ice growth and retreat (Ducklow et al., 2012; Pirtle-Levy, 2016). Phytoplankton and zooplankton rely on seasonal ice conditions for their sustained growth and development. These planktonic organisms serve as the foundation of the overall food web on the WAP shelf (Ducklow et al., 2013; Cape et al., 2014). Ultimately, organic matter from the pelagic food web rains down onto the sea floor, providing nutrition to the benthic ecosystem creating benthic “foodbanks” (Mincks et al., 2005).

Regional climate (and sea-ice) influences both the biogenic and lithogenic components of particle flux. Lithogenic flux originates from coastal discharge of terrestrial sediment that can become resuspended via tidal currents and wind induced circulation, creating a nepheloid layer and facilitating seaward transport (Hillenbrand et al., 2003; Khim et al., 2007; García et al., 2011). On the inner WAP shelf, surface gyres can transport suspended fine-grained particles southward of their original location. Net bottom transport is seaward as noted from sediment cores and clay provenance studies along the WAP (Hillenbrand et al., 2003). The interplay between the glaciological setting and shelf circulation around the WAP drive the lithogenic component of particle flux (Hillenbrand et al., 2003), which is mainly derived from terrestrial sources, e.g., sub-glacial runoff, ice sheet basal flow, and ice-rafted debris (Harden et al., 1992; McGinnis et al., 1997; Khim et al., 2007;García et al., 2011 ; Weston et al., 2013). The lithogenic flux is enhanced during the relatively warmer spring and summer seasons along the peninsula (García et al., 2011; Weston et al., 2013).

Given the decline in sea-ice duration over the past few decades (Stammerjohn et al., 2008) and the tightly coupled interaction between pelagic productivity and benthic food webs (Mincks et al., 2005), it was postulated that changes in the pelagic ecosystem function and structure would translate into changes in the benthic environment. To test this hypothesis, the second phase of the FOODBANCS Project, FOODBANCS2, was initiated. The focus of FOODBANCS2 research was to observe and document changes in the benthic environment along a climatically sensitive, N-S transect on the WAP shelf that exhibited a gradient in sea-ice duration (Smith et al., 2012; Figs. 1 and 5). Investigators proposed to examine particle/radionuclide flux dynamics and benthic ecology in the context of changes in sea-ice coverage for this sensitive, high-latitude environment.

There have been numerous flux studies employing particle traps along the peninsula, e.g., FRUELA96 (Anadón and Estrada, 2002; Palanques et al., 2002), the Palmer LTER (Ducklow et al., 2012) and FOODBANCS (McClintic et al., 2008; Smith et al., 2008b). However, particle traps may under-sample both in time and space (Buessler et al., 2010), as well as miss near-bottom lateral transport. Consequently, the net flux to the benthic environment in some cases may have substantial uncertainties and be poorly understood. In order to get a better understanding of particle and radionuclide fluxes, sediment cores were retrieved to examine particle/radionuclide flux dynamics along the WAP, because the seabed is the ultimate integrator of net seafloor fluxes.

To evaluate the influence of climate change on the WAP and to understand the nature of particle flux over a range of time scales, a suite of radiochemical tracers (^{230}Th, ^{14}C, ^{210}Pb and ^{234}Th) with variable half-lives (75.2 ky, 5730 y, 22.3 y and 24.1 days, respectively) were measured on sediment samples from several shelf locations (shelf depths between 500 and 600 m), where fine-grained sediment accumulates. By comparing the distributions of these tracers in the seabed, the effects of regional warming on the Antarctic Peninsula over the past few decades can be resolved from long-term conditions extending back centuries to millennia.

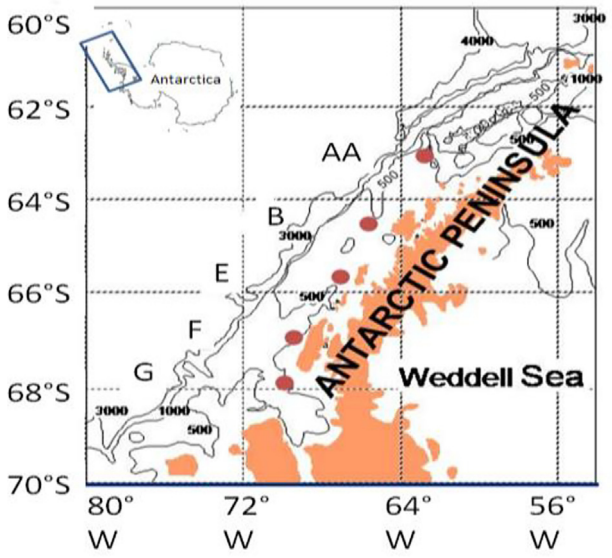

Fig. 1. Map of study sites for FOODBANCS-2 Project. Contour lines represent shelf bathymetry. Stations (shown as red dots) were occupied during Austral Summer and Winter 2008, and Austral Summer 2009.. (For interpretation of the references to colour in this figure legend, the reader is referred to the web version of this article).

The goal of this research is to evaluate trends in the radio-isotopic flux/inventories of four particle flux proxies, and to test the hypothesis that the southernmost stations along the 550 km N-S WAP transect are exhibiting enhanced particle fluxes (comparable to the northernmost stations). Specifically, it is hypothesized that the inventories of ^{234}Th (characterizing monthly time scales) collected from the southernmost stations, during 2008 and 2009, are suggestive of a temporal increase in particle flux relative to the northern stations of the transect and the long-term (centurial to millennial) trend of decreasing particle flux with increasing latitude. The underlying expectation is that as warming occurs along the West Antarctic Peninsula, there should be an increase in particle flux, both lithogenic and biogenic, as a consequence of increasing erosion of continental sediments and pelagic production.

2. Methods

2.1. Study sites

The WAP was sampled along a 550 km N-S transect between 63˚S and 68˚S (Fig. 1). Three cruises were completed using the RV Lawrence M. Gould during the austral summers of 2008 and 2009 and the RV Nathaniel B. Palmer during the austral winter of 2009. Cruises were timed to coincide with periods of highest and lowest primary production (and presumably particle flux), summer and winter, respectively. Five stations were selected along the WAP shelf, each at water depths of ~600 m (where the seabed accumulates fine-grained sediments). Station selection coincided with a natural gradient in sea-ice coverage and duration (Smith et al. (2012)): Station AA, the northernmost station, on average ice-free > 9 mo per year, in contrast to Station G, the southernmost station, ice free ~3 mo per year of the year from 2004 to 2008

(Smith et al., 2012). Stations were occupied multiple times during each cruise, and each time a station was occupied, a megacore with 12 tubes, each 10-cm diameter, was collected.

Cores with the least disturbed sediment-water interfaces were sampled for radiochemical analysis at 0.5-cm intervals down to 2 cm, every centimeter from 2 to 10 cm, every other centimeter from 10 to 20 cm and at 2-cm intervals from 20 cm to the bottom of the core. A Kasten core was also collected at each of the five stations and subsampled over 3-cm depth intervals at 5–8 depths throughout the 1–3 m cores. Sediments used to measure ^{14}C were dried at 100 °C aboard ship. All other radiochemical samples were stored at 4 °C and dried just prior to analysis. Three to five megacore tubes from each station on each cruise were analyzed for ^{234}Th activity. ^{210}Pb was measured on one core from each station per cruise (3 total per station). ^{230}Th analyses were run on four Kasten cores (Stations AA, B, F, and G).

2.2. Radiochemical analysis

Analyses for ^{234}Th, ^{210}Pb, and ^{230}Th were accomplished by chemical digestion of approximately 5 g of dried, homogenized sediment in near-boiling 6 M hydrochloric and 7 M nitric acids, following the methods of Aller and DeMaster (1984). All three radiochemical analyses were made on separate subsamples of sediment from the same core. An analyte-appropriate spike of known activity was introduced prior to initial digestion: ^{230}Th (for ^{234}Th), ^{209}Po (for ^{210}Pb) and ^{228}Th (for ^{230}Th). For analyses of thorium isotopes and their uranium parents, thorium and uranium fractions were isolated after initial digestion using anion exchange (AG1-X8, 200-400 mesh, Cl^- form) techniques. Thorium and uranium activities were further purified using 0.4 M thenoyltrifluoroacetone (TTA - in benzene) extractions followed by dry deposition onto stainless steel planchettes on a heated chimney (Aller and DeMaster, 1984). Activities of ^{232}Th, ^{230}Th, and ^{228}Th were determined using alpha spectroscopy, whereas the activity of ^{234}Th was determined via anti-coincidence beta counting. ^{210}Pb analyses were made by isolating its granddaughter, ^{210}Po, in 1.5 M HCl, followed by deposition of the polonium isotopes on 1-cm^2 silver planchettes. After plating, samples were counted using surface barrier detectors and alpha spectroscopy. The statistical uncertainties inherent in observing decay events were propagated throughout the various data calculations.

For both thorium isotopes, the uranium parent was directly measured, but for ^{210}Pb, the activity of the effective parent (^{226}Ra) was approximated by determining the asymptotic activity of the total ^{210}Pb activity profile at depth. To understand particle flux along the peninsula, inventories of excess activities for each of the three radioisotopes were calculated using the equation:

$$I = \sum A^{*}\rho_{db}\Delta z \quad (1)$$

where A^* is the excess activity at depth interval Δz and ρ_{db} is the dry bulk density (Table 1). Under steady-state conditions, the radiochemical flux of a particular radioisotope to the seabed can be calculated by multiplying the seabed inventory by its radioactive decay constant.

The magnitude of observed radiochemical fluxes often can be used to resolve the relative contributions from vertical settling and from lateral transport. The production of each tracer in the water column from a dissolved, long-lived parent is relatively well known and a function of water depth; therefore, a focusing factor (Psi) can be derived by comparing observed seabed fluxes to the expected water column production for a particular radioisotope (Bacon, 2004). Values equal to one indicate vertical settling is the predominant component of sediment flux. Values greater than one indicate contributions from both vertical settling and lateral transport to the sediment flux. Values less than one indicate that the tracer is transported laterally away from the station area (or for isotopes with short half-lives, as is the case for ^{234}Th, decay within the water column).

^{14}C activity was determined on the organic-carbon fraction of Kasten-core sediments. Particulate inorganic carbon was removed using an overnight, 1 M HCl aqueous pretreatment. Thirty to 90 mg of pretreated sediment were combusted on an elemental analyzer (Flash EA 1112), followed by CO_2 isolation into glass tubing using cryogenic techniques (Purinton et al., 2008). The CO_2 samples were analyzed for ^{14}C activity using the accelerator mass spectrometer at the NOSAMS facility (Woods Hole Oceanographic Institution). $^{14}C_{org}$ ages were calculated by multiplying the natural log of the ^{14}C fraction modern value (corrected for ^{13}C variations) by 8267 years. Sediment accumulation rates were determined from the least squares fit of a ^{14}C age versus depth profile (Fig. 2). Geochemical data were handled as discrete observations and arithmetically averaged when pooled values were used in statistical analyses. For seasonal and annual trends, ^{234}Th data were pooled for each station and evaluated spatially and temporally using a linear model, treating both station (spatial) and cruise (temporal) effects as fixed.

2.3. Sea-ice metrics

Annual sea-ice trends along the WAP were evaluated from the Bootstrap-2 passive microwave dataset available through the National Sea Ice Data Center (NSIDC) in Colorado for the interval 1979–2009. The five stations were geo-coordinated with Interactive Data Language (IDL) using the modified source code provided by NSIDC. A single 25 km^2 cell of the satellite data matrix represented each of the five stations. Binary satellite data were input into Matlab and the resultant daily concentrations were used to derive the sea-ice statistic used in this study. The parameter of interest, sea-ice free days, was quantified by counting the number of days that had ice concentrations less than 15% (Stammerjohn et al., 2008). For annual trend analysis, a year was defined as occurring from March 15th of the initial year to March 14th of the subsequent year. Due to incomplete data, 1987 was excluded from the analyses.

To evaluate seasonal trends in sea-ice coverage at each station and spatial trends per cruise (FB2-x), the sea-ice free days were counted for the 120 days (approximately 5 half-lives of the shortest lived tracer, ^{234}Th) prior to collection of each megacore sample. The ratio of observed sea-ice free days out of 120 was treated as binomial count data and run as a generalized linear model, treating both station and cruise as fixed effects. The ratios of ice-free days out of total days were log-rhythmically transformed in order to account for the use of count data when evaluating ice trends. All statistical analyses were performed using SAS v. 9.4 at the alpha significance level of 0.05.

3. Results

3.1. Millennial trends

The sedimentary distribution of ^{14}C in Kasten cores is not influenced to a significant extent by particle mixing (bioturbation) (Harden et al., 1992); therefore, this long-lived radioisotope is an effective tracer of sediment accumulation rates (SAR) on the WAP shelf. ^{14}C ages near the top of the Kasten cores (Fig. 2) ranged from 2300 to 3900 years, in part because of the high reservoir age (1300–1500 years: average pre/post-bomb reservoir age of 1300 ± 100y - Berkman and Forman, 1996) of plankton as a result of high-latitude upwelling and also presumably because of lateral transport of aged organic matter down into these shelf basins. The ^{14}C sediment accumulation rates ranged from 67 cm/ky at Sta. AA, to 28 cm/ky at Sta. B, to 22 cm/ky at Sta. E, to 5.6 cm/ky at Sta. G.

The calculated SARs assume that the surface age of bulk organic matter is constant over time. The sediment accumulation rates decrease from N to S along the transect, and there is an 11-fold greater flux of sediment, on millennial time scales, at Station AA compared to Station G (Fig. 3). The SAR for Station F was not reported due to an unresolved,

Table 1
Geochemical results from radioisotopic analyses.

Station	^{230}Th		^{14}C		^{210}Pb				Ice-free Days	^{234}Th					
	Inventory	error	SAR	error	Inventory	error	mean	D_b		D_b	Inventory	error	Cruise	cruise	annual
	(dpm/cm^2)	(±)	(cm/ky)	(±)	(dpm/cm^2)	(±)		(cm^2/y)		(cm^2/y)	(dpm/cm^2)	(±)		Mean	mean
AA	0.3*	0.1	67	17			184.3 (13.3)		120	2.7	2.4	0.1	2–1	5.5 (2.1)	11.2 (2.5)
					175.5	2.3		0.1	120	2.7	5.9	0.1			
									120	3.4	8.2	0.1			
									120		5.1	0.1			
									120	8.6	6.3	0.1			
									120		2.2	0.1	2–2	3.9 (1.5)	
									120	1.0	4.4	0.1			
					199.6	2.9		0.1	120	2.1	5.0	0.2			
									120	35.1	11.6	0.2	2–3	9.0 (2.4)	
					177.7	2.0		0.4	120	8.5	8.6	0.2			
									120	6.5	6.9	0.1			
B	4.4**	0.3	28	24	70.3	2.8	84.2 (12.3)	0.3	120	1.4	2.4	0.1	2–1	1.9 (1.4)	5.1 (2.1)
									120	3.3	4.0	0.1			
									120	3.0	1.4	0.1			
									120		1.2	0.1			
									120		0.5	0.0			
									119	1.3	1.7	0.1	2–2	1.7 (1.2)	
					88.7	2.0		0.8	119	4.4	3.4	0.1			
									119	1.8	1.0	0.1			
									119		0.7	0.0			
					93.7	2.0		0.1	120	6.3	2.2	0.1	2–3	4.9 (1.5)	
									120	12.2	5.7	0.1			
									120	4.8	4.9	0.1			
									120	16.8	6.0	0.2			
									120	1.8	5.6	0.2			
E	ND		22	17	65.4	1.7	65.2 (4.4)	0.3	119		1.3	0.0	2–1	0.4 (0.8)	2.8 (2.5)
									116		0.0	0.0			
									116	1.8	0.0	0.0			
					69.4	2.6		0.4	114		0.8	0.0	2–2	0.6 (0.2)	
									114		0.6	0.0			
									113	0.4	0.4	0.0			
									120	4.5	4.9	0.1	2–3	4.0 (0.9)	
									120	6.5	3.1	0.1			
					60.7	1.7		0.5	120	7.9	4.0	0.1			
F	7.2	1.6	ND				66.4 (26.9)		120	1.1	5.1	0.1	2–1	2.1 (2.7)	11.5 (10.0)
									118	2.4	1.2	0.0			
					97.3	2.6		1.6	118		0.0	0.0			
									107		2.2	0.1	2–2	2.3 (0.7)	
									106		3.0	0.1			
					53.8	2.9		1.7	106		1.7	0.0			
					48.1	2.3		0.9	119	6.5	11.8	0.1	2–3	16.3 (5.4)	
									119		14.6	0.1			
									119	1.0	22.3	0.1			
G	30.2	1	6	3			46.1 (13.9)		102		1.2	0.0	2–1	4.0 (2.4)	9.5 (3.6)
									102	10.9	2.7	0.1			
					33.1	0.9		0.4	102		7.1	0.3			
									103		3.1	0.1			
									103	2.0	5.8	0.1			
									104	2.0	2.8	0.1	2–2	2.9 (0.9)	
									104	1.6	2.5	0.1			
					64.2	1.8		0.8	103	0.9	4.5	0.1			
									103	3.9	2.8	0.1			
									102	1.2	2.1	0.0			
									100	137.0	16.1	0.1	2–3	9.1 (5.1)	
					37.5	0.7		0.9	100	6.2	6.1	0.1			
					49.4	1.3		0.5	100	1.2	4.9	0.1			
									100	10.1	12.9	0.1			
									100	3.0	5.5	0.1			

Cruise information: 2–1 is Summer 2008, 2–2 is Winter 2008 and 2–3 is Summer 2009. Absolute error was determined primarily from counting statistics. Annual mean ^{234}Th inventories presume the winter contribution was the same for 2008 and 2009. For calculated mean inventories, parenthetical values represent standard deviations (1σ). ND = not determined.

* ^{230}Th activities from Station AA were at detector limits and were not considered when evaluating trends along the WAP.

** ^{230}Th data from Station B were interpolated from 0 to 10 cm.

down-core ^{14}C sediment profile.

^{230}Th inventories, listed in Table 1, were integrated to the bottom of the Kasten core (Stations AA, B and F) or to a depth horizon of approximately 7ky (Station G). Excess activity was very small (near detector limits) for Station AA, probably due to the high sediment accumulation rate and subsequent dilution of the thorium signal. Station G had the highest (measurable) inventory, 31.6 dpm/cm^2, and Station AA the lowest, 0.2 dpm/cm^2. There was an increase in inventory along

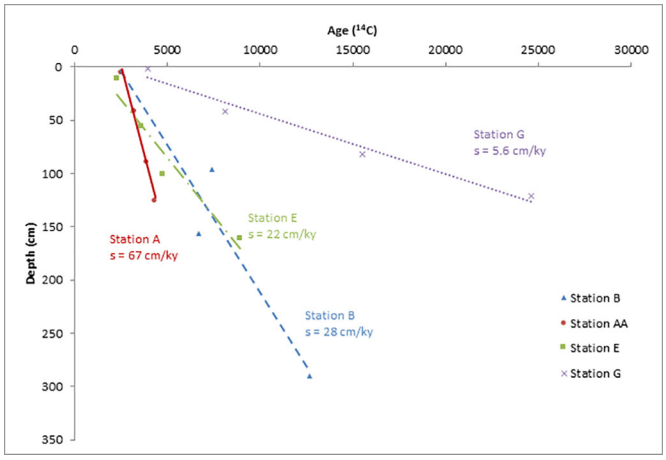

Fig. 2. Plot of $^{14}C_{org}$ age (non-Libby) as a function of depth in the seabed for 4 West Antarctic Peninsula stations. Accumulation rates vary by an order of magnitude and decrease southward. The analytical uncertainty in the ^{14}C ages (typically 30 years) is smaller than the size of the symbol used to represent the data point in this figure.

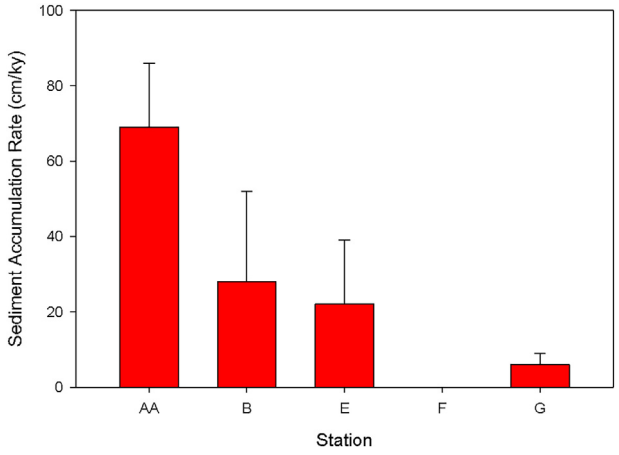

Fig. 3. Sediment accumulation rates (SAR) along the 550 km N-S transect. On millennial timescales, there is decreasing particle flux as distance from AA (farther south) increases. Error bars represent the 95% confidence limits on the SAR from linear regression. The linear regression of sediment accumulation rate versus distance along the N/S transect (beginning with Sta. AA) has an R-squared value of 0.88, p-value = 0.062.

the transect southward of Station AA, which can be attributed to the increased time interval over which the sampled sediments at the southern stations (especially Station G) integrated, because of southwardly decreasing sediment accumulation rates (67 cm/ky at Station AA versus 5.6 cm/ky at Station G – Table 1).

^{230}Th, which is highly particle reactive, is produced at a constant rate from its more soluble parent, ^{234}U. ^{230}Th has a short residence time in the water column (< 40 years in deep water) relative to its half-life (Francois et al., 2004). These properties result in the nearly complete scavenging of ^{230}Th from the water column. ^{230}Th inventories were used to calculate a sediment-focusing factor (Psi) following the method of Francois et al. (2004), based on the formula:

$$\psi = \int \frac{A^* \rho_{db} z}{\beta_{230} hs} \quad (2)$$

where A* is the age corrected excess activity of the depth horizon z, rho is the dry bulk density, β_{230} is the water column production of ^{230}Th over water depth h, and s is the dated age of depth horizon z. Age correction and tie-points used in the Psi calculation were based on ^{14}C sediment accumulation rates. In the calculation of Psi, ^{230}Th activity was only integrated to a time horizon of at most 7 thousand years, a period of relatively uniform sedimentation in this high-latitude environment (Heroy and Anderson, 2007; Bentley et al., 2011). Stations AA and B had Psi values > 2, suggesting that sediment focusing plays a substantial role at the northern stations. Southern stations had ^{230}Th Psi values slightly greater than one (1.3–1.6), suggesting vertical particle scavenging predominates and less lateral transport and focusing of sediment (Table 2).

Table 2
Focusing factors (Ψ) for ^{230}Th, ^{210}Pb, and ^{234}Th.

Station	$^{230}Th_{xs}$	$^{210}Pb_{xs}$	$^{234}Th_{xs}$
	Observed	Observed	Observed
	Ψ	Ψ	Ψ
AA	2.4	22.0	0.014–0.078
B	2.2	10.0	0.003–0.040
E	na	7.8	0.003–0.033
F	1.5	7.9	0.008–0.151
G	1.3	5.5	0.008–0.109

^{230}Th Psi values were calculated based on a water column production rate of 26.7 dpm m^{-3} ky^{-1} (Francois et al., 2004). The estimated ^{226}Ra activity in the water column was 0.14 dpm/kg (Ku and Lin, 1976), and the estimated ^{238}U activity was 2.4 dpm/kg (Pilson, 2012). ^{234}Th Psi ranges were based on the minimum and maximum observed inventories. na = not analyzed.

3.2. Decadal-centurial trends

^{210}Pb, with a 22.3 year half-life, can be useful in understanding sedimentary processes over ~110 years, i.e., five half lives (Table 1). There was a southward decrease in radiochemical inventory/flux along the transect from Station AA (mean inventory of 184 dpm/cm^2) to Station G (46.1 dpm/cm^2, Table 1 and Fig. 4). Stations E and F had similar inventories of 65.2 and 66.4 dpm/cm^2, respectively (Table 1). At Station AA, one near-surface sample had an activity of 150 dpm/g, which was higher than any other recorded activity in the samples. If this sample were excluded from the inventory calculations as an outlier, the conclusions drawn from the statistical tests remain the same; therefore, the sample was included in the final analysis. ^{210}Pb inventories were significantly different among the stations (one-way ANOVA, n = 16, p-value < 0.0001). The post-hoc test Tukey multiple comparisons test showed that the mean ^{210}Pb inventory at Station AA

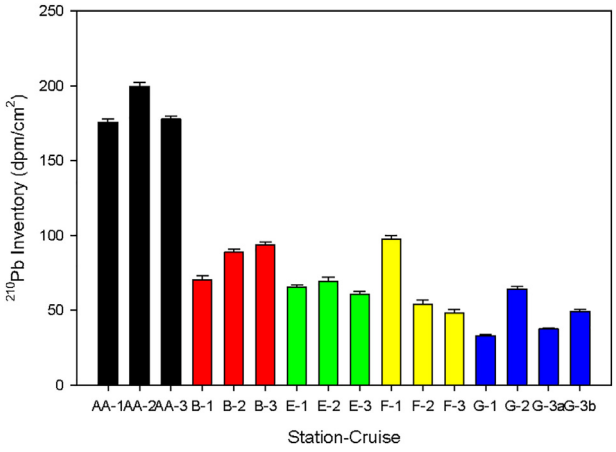

Fig. 4. ^{210}Pb inventories from all sampled cores denoted by Station-FOODBANCS cruise, e.g., AA-2 is Station AA cruise FOODBANCS2–2. Station G had 2 cores (a and b) analyzed from cruise FOODBANCS2–3. Error bars represent absolute errors (calculated from counting statistics).

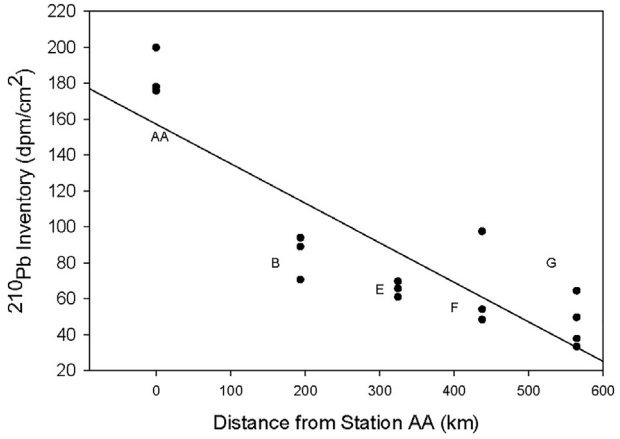

Fig. 5. ^{210}Pb inventory weighted regression analysis. The centurial trend is that of decreasing radiochemical flux to the seabed from north to south (R^2 = 0.81; *p*-values < 0.0001).

was significantly different than the other 4 stations' means (p-value < 0.0001). There is a significant trend of decreasing ^{210}Pb inventory from north to south (Fig. 5, R^2 = 0.81; *p*-value < 0.0001).

3.3. Seasonal patterns

Due to its short half-life of 24 days, ^{234}Th is an excellent tracer for radiochemical flux and particle dynamics over seasonal timescales (~120 days). For cruise FOODBANCS2–1, mean ^{234}Th inventories ranged from 0.4–5.6 dpm/cm^2. There was a decrease in inventory from Station AA to E followed by an increase in inventory at Stations F and G (Fig. 6). Mean ^{234}Th inventories from FOODBANCS2-2 (Austral winter) ranged from 0.6–3.9 dpm/cm^2. Mean inventories exhibited the same latitudinal pattern as observed the previous summer. Summer 2009 (FOODBANCS2-3) had ^{234}Th inventories as high as 22.3 dpm/cm^2 at Station F, and as low as 4.0 dpm/cm^2 at Station E; the same general pattern observed during the previous two cruises was observed during cruise FOODBANCS2-3 (Table 1 and Fig. 6).

A two-way ANOVA test showed a significant interaction between Station and Cruise effects (n = 56; *p*-value = 0.03); therefore, the main effects of the Station (on ^{234}Th inventory) depended upon the cruise. In fact, ^{234}Th inventories did not differ significantly along the transect

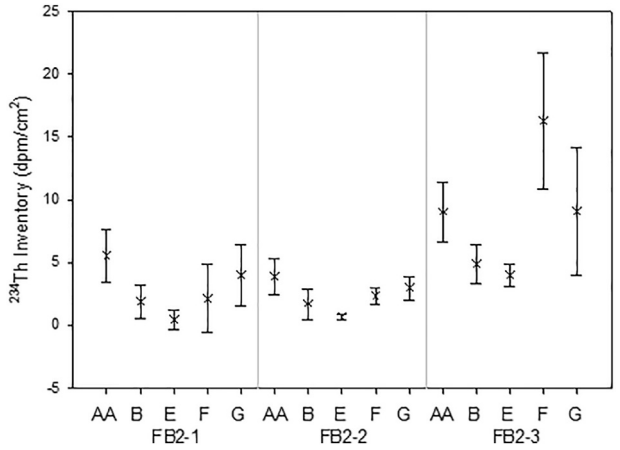

Fig. 6. ^{234}Th inventories from the three FB2 cruises. Points are mean core inventories (n = 5) and error bars are standard deviations of the means. Each cruise (season) had decreasing inventories from Stations AA to E, but increased inventories from E to G. Cruise FOODBANCS2-3 (Summer 2009) had higher inventories than either previous cruise, consistent with documented inter-annual variability in ^{234}Th (McClintic et al., 2008).

during cruise FB2-1 or FB2-2. Post-hoc Holm-Sidak multiple comparison showed that Cruise FB2-3 ^{234}Th data were significantly different from Cruises FB2-1 or FB2-2 (*p*-values < 0.001).

Seasonal variability in particle flux has been well documented along the WAP (McClintic et al., 2008; Smith et al., 2008b; Buessler et al., 2010; Ducklow et al., 2012). Although the magnitude of the ^{234}Th inventory differed from season to season, consistent station to station patterns in the inventory (high-low-high) were observed during the 12-month study period (Fig. 6). For the WAP, the inventories were approximately the same along the N-S transect during each cruise. There was no statistically significant linear trend along the transect for any of the three cruises (weighted linear regressions, *p*-values > 0.132).

3.4. Annual patterns

Annual ^{234}Th inventories were calculated based on the assumption that the winter inventory (FOODBANCS2-2) was constant from year-to-year; i.e., the 2008 inventory is equivalent to FOODBANCS2-1 plus FOODBANCS2-2 inventories and the 2009 inventory equals the FOODBANCS2-2 plus FOODBANCS2-3 inventories. Annual ^{234}Th inventories were highest at Station AA for 2008 (9.4 dpm/cm^2) and highest at Station F for 2009 (18.6 dpm/cm^2). For both 2008 and 2009, inventories were lowest at Station E (1.1 and 4.6 dpm/cm^2, respectively), and increased away from Station E, both northward and southward (similar to the observed seasonal patterns – Fig. 6). The observed inventories at every station for Summer 2009 were the same as or greater than ^{234}Th inventories for all of 2008. There was no statistical trend in annual ^{234}Th inventories N-S with distance along the transect (R^2 = 0.014; *p*-value = 0.192).

3.5. Sea-ice patterns

Table 1 shows the counts of ice-free days for the 120 days prior to sediment core retrieval. The number of ice-free days observed were lower in the winter compared to the summer for southern Stations E, F and G. Stations AA and B were ice-free for the previous 120 days regardless of season. Over all, Station G had the fewest ice-free days observed for every cruise. Based on satellite ice patterns, Stations B, E, F and G had an apparent increase in the number of ice-free days over the 29 years prior to 2008. Stations E, F and G showed the largest percentage increase in ice-free days (62%–94%) relative to the natural decrease in ice-free days with increasing latitude.

No statistical correlation existed between ice-free days and ^{234}Th inventories, based on pooled inventories from the three cruises (excluding observations of zero inventories) across stations (n = 56, *p*-value = 0.147). However, at station E and G, a correlation between ice-free days and station ^{234}Th inventory was observed (Fig. 7). The ^{234}Th inventory at Station E increased as ice-free days increased (*p*-value = 0.013 – Fig. 7). Station G had a statistically significant decrease in ^{234}Th inventory as the number of ice-free days increased (*p*-value = 0.019 –Fig. 7). Station F demonstrated no statistical correlation (Fig. 7, *p*-value = 0.326) between observed inventory and the number of ice-free days, likely due to the large difference in ^{234}Th inventory between summer 2008 and 2009, sampling timing, and/or variation in sea-ice concentration during "ice-free" (0–15%) and ice-covered (15–100%) conditions (see discussion).

4. Discussion

4.1. Radiochemical patterns

In any marine environment, there are two main components of particle flux to the seabed – vertical settling and lateral transport. The vertical component is derived from particulate matter settling vertically through the water column overlying the seabed. Laterally transported sediment comes from outside the study area, and transport is generally

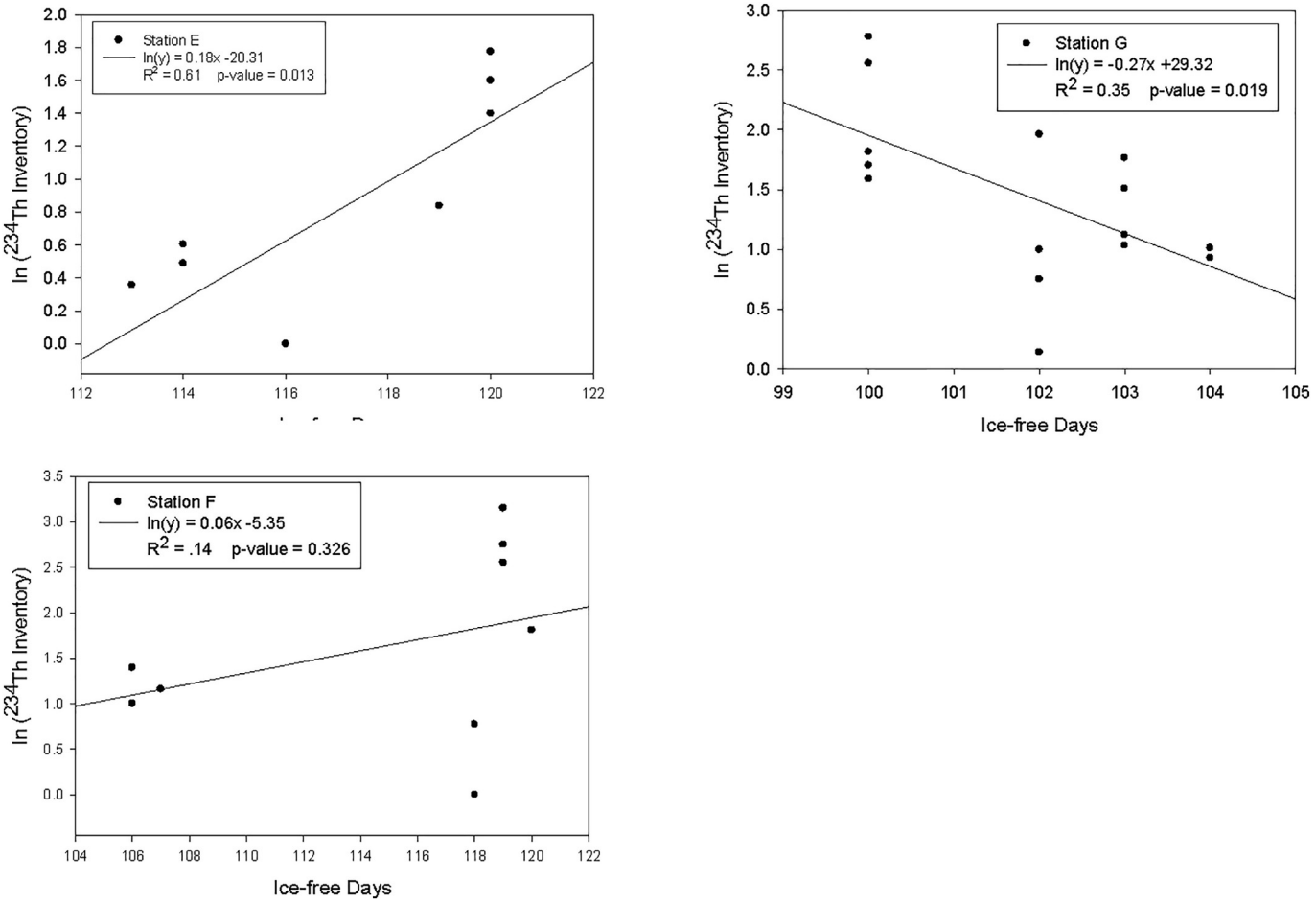

Fig. 7. The log-transformed ^{234}Th inventories at Station E, Station F and Station G relative to ice cover 120 days prior to core recovery for all three cruises. Station E showed a positive, linear trend between ^{234}Th inventory and ice-free days. Station G, however, had a negative linear trend. Station F showed high inter-annual variability between summer 2008 and 2009 and thus no correlation between ice-free days and ^{234}Th inventory.

accomplished via currents, tides and (in shallower environments) waves. The seabed acts to integrate these sources.

The ^{230}Th data suggest that sediment has been accumulating at all stations on millennial timescales (Table 2). Estimates of sediment focusing at the northern station are approximate due to the high sediment accumulation rate at Station AA, leading to excess ^{230}Th activities near detection limits. The ^{230}Th data suggest that sediment flux over millennial timescales (1-7ky) effectively scavenges all of the thorium from the overlying water column. The observed inventories provide some supportive evidence for sediment focusing and lateral transport via currents on long-term time scales consistent with ADCP derived physical oceanographic data reported for the Peninsula area by Savidge and Amft (2009) and Moffat et al. (2008). A portion of the sediment flux at Station AA, with a ^{230}Th Psi value > 2 (Table 2), is likely attributable to focusing via lateral transport. Sediment focusing within the Bransfield Strait has been documented in the past (Palanques et al., 2002). The ^{230}Th Psi values near one (Table 2) along the southern reaches of the WAP transect indicate that vertical scavenging of particle has predominated and that minimal ^{230}Th has been supplied from surrounding waters, i.e., very little net lateral transport has occurred on millennial timescales. The lack of lateral transport on millennial timescales indicates that ^{230}Th inventories in the seabed are not sensitive to recent changes in climate and particle flux as suggested by Smith et al. (1999), who describe a warmer, maritime climate moving southward along the Peninsula over the past several decades.

The ^{14}C-derived sediment accumulation rates (SARs) decrease along the N-S FOODBANCS-2 transect (Table 1;Figure 8), coincident with the natural sea-ice gradient along the Peninsula (Smith et al., 2012). SARs decreased from Station AA (67 cm/ky) through Station B and E (28–22 cm/ky) to Station G (5.6 cm/ky) along the 550 km N-S transect (R^2 = 0.88; p-value = 0.062) Similarly, ^{210}Pb inventories statistically decreased along the WAP transect from north to south as shown in Figs. 4 and 5 (p-value < 0.001). The predicted ^{210}Pb inventory (Ψ = 1) can be calculated based on the water column activity of its effective parent, ^{226}Ra (see Table 2 above), and the overlying water column height (yielding a value of ~8.0 dpm/cm^2 for a water depth of ~600 m which is ~20 times less than the observed average ^{210}Pb sediment inventory at Station AA). The water-column path length necessary to support the observed ^{210}Pb inventories along the WAP transect ranged from 3 to 14 km (compared to the actual water depth of ~600 m). Clearly, there is a significant mechanism by which excess ^{210}Pb is laterally transported to all of the WAP study sites on 100-year time scales.

Due to its 22.3y half-life, approximately half of the observed ^{210}Pb inventories (and resultant Psi values > > 1) along the WAP can be attributed to sedimentary process occurring before 1979. It is conceivable that the inventories indicate a diminished impact from climate change effects; however, the climate record may not go back far enough to determine long-term relationships between sedimentary processes and climate change effects. The high inventories likely reflect the water depth and the fine-grained sediments of the study area, as well as circulation dynamics on the shelf. Fine grained sediments (those more likely to scavenge radiochemical tracers from the water column) tend to accumulate below 400 m on the WAP shelf (Harden et al., 1992). The sediments occurring at water depths < 400 m are primarily reworked

sands containing very little or no fine-grained sediment (and thus, very low abundance of particle reactive tracers such as ^{210}Pb). Approximately 30% of the total shelf area along the WAP has water depths in excess of 400 m. Therefore, scavenging of the nearby, shallow-shelf environment's ^{210}Pb (from water column production) can explain a ^{210}Pb Ψ value of approximately 3.

In addition, the high ^{210}Pb inventories and large Psi values can (in part) be explained by the short (relative to the half-life of ^{210}Pb) residence time of the waters along the WAP, as part of regional circulation. Harden et al. (1992) reported a residence time for Marguerite Bay of approximately 8y and as short as 2y for the Gerlache Strait. The 100-year timescale integrated by ^{210}Pb is sufficiently long compared to the water's residence time that ^{210}Pb produced in offshore waters (where particle flux is very low) has time to be transported onto the shelf, where it can be scavenged by the enhanced fluxes of fine-grained sediment (lithogenic and biogenic) occurring on the shelf and deposited in the shelf basins (acting as localized depocenters).

In the Bransfield Strait, subglacial discharge is highest during the spring-summer melt, forming sediment-rich plumes (Harden et al., 1992). These plumes move seaward via tidally induced resuspension events and density flows (Masqué et al., 2002; Isla et al., 2004; Cape et al., 2019). Continued warming trends would likely elevate the sediment load in this region (Cape et al., 2019) resulting in enhanced particle scavenging, which would lead to future increases in seabed inventories of ^{210}Pb.

Within Marguerite Bay, sediment is mainly lithogenic in origin and glaciomarine processes control its distribution and rate of accumulation (McGinnis et al., 1997; Hillenbrand et al., 2008). Intrusions of warmer circumpolar deep water (CDW) have been shown to increase ice-shelf melt, resulting in increased suspended sediment concentrations (Taylor et al., 2001; Gilbert et al., 2003; Cape et al., 2019). Again, further warming within Marguerite Bay could lead to increases in sediment load to the water column (lithogenic and biogenic). Coupling the short residence time of water parcels within Marguerite Bay to an increased sediment load would tend towards increasing the seabed inventories of ^{210}Pb in the future.

As sea-ice melts it produces a freshwater lens, promoting stratification and subsequently enhancing primary productivity (Smith and Nelson, 1985). Increased atmospheric temperatures and subsequent higher wind intensities have made the WAP sea-ice season shorter (Stammerjohn et al., 2008). Smith et al. (2008a) showed that the decrease in the sea-ice season has the potential to increase the rates and duration of primary production along the WAP. Indeed, southern WAP productivity has increased in recent years (Montes-Hugo et al., 2009). It is reasonable to presume that as warming trends continue, particle flux will increase due to the increased water column productivity. Coupled with the potential lithogenic material increase from increased basal flow, subglacial runoff and resuspension, the higher sediment load will effectively scavenge more particle reactive tracers from the water column, increasing seabed inventories. Such enhancement to the radiochemical signal could help to explain the apparent lack of a monotonic trend in ^{234}Th inventories N-S.

The data from the N-S transect showed similar ^{234}Th inventories for a given station from both FOODBANCS2–1 and FOODBANCS2–2, i.e., the austral summer and winter of 2008, respectively (Fig. 6). There was no statistical difference in inventories between the two seasons (p-value = 0.812). The flux to the seabed observed at Station B during winter 2008 (488 dpm/m^2/d) was similar to that observed at a nearby near-bottom sediment trap deployed during the summer of 2000 (400 dpm/m^2/d - McClintic et al., 2008). Presumably, little primary production occurs in the winter; as such, the observed winter inventories would more likely be explained by the resuspension and lateral transport of lithogenic material from other locations.

The range in the observed mean ^{234}Th sediment inventories at the 5 stations during the 3 cruises (1.1 to 19 dpm/cm^2) can be explained by complete scavenging of 5–80 m of water column, or incomplete scavenging of a taller column. During the winter seabed inventories are likely the result of more complete scavenging of particles in near-bottom waters. During the spring and summer, much of the ^{234}Th produced in the euphotic zone is likely to be scavenged by the organic matter sinking out of the surface waters. However, significant particulate organic matter is recycled at depth (releasing the associated ^{234}Th), i.e., scavenging during the summer is likely to occur in a vertical mode over a greater part of the water column (but at much less than 100% removal). Thus, with very different modes of scavenging and tracer transport during the different seasons, it is likely fortuitous that the winter and summer ^{234}Th inventories were similar. It should also be noted that during the spring and summer sampling periods, much of the ^{234}Th signal produced in surface waters may reside temporarily on particles suspended in the water column (and not in the seabed), especially during plankton blooms.

In summer 2009, the southern stations (F and G) had the highest ^{234}Th inventories (10-fold greater than summer 2008), and indicated substantial inter-annual variability on the WAP (McClintic et al., 2008; Smith et al., 2008a; Buessler et al., 2010). In contrast, the ^{234}Th inventories at Stations AA and B were nearly constant during these two summers. The high ^{234}Th inventory observed at Station G during the summer of 2009 corresponded with some of the lowest number of ice-free days at this station. The high inventory at G may be explained in part by the timing of the ice-edge retreat at the station (sampling at Station G occurred at or near the ice edge, enhancing biogenic particle flux, Smith and Nelson, 1985), and not the absolute number of ice-free days (Fritsen et al., 2011). During the summer of 2009, Station F exhibited the highest ^{234}Th inventories observed in the study. In contrast to Station G (which had only 100 ice-free days prior to sampling, out of 120), Station F had 119 days of ice-free conditions (of 120) prior to sampling.

The mean ^{234}Th inventories at Station F during FOODBANCS2–3 were (nearly) twice as high as at Station G during the same period. The enhanced ^{234}Th seabed inventories (and by analogy particle flux) observed at Station F relative to Station G is consistent with a longer time-period of open-ocean conditions and the likelihood that Station F was near the ice edge for an extensive and longer period of time (perhaps 2–3 weeks) than Station G.

The sea-ice data (along with the ^{234}Th sediment inventories) suggest that the northern stations AA and B may not have been greatly influenced by changes in sea-ice duration or the timing of the ice-edge retreat in recent years. However, the ^{234}Th inventories at Stations F and G are consistent with the idea that particle flux is increasing, possibly in response to the climate shift and the changing sea-ice dynamics along the peninsula.

4.2. Summary of temporal patterns in particle flux

Millennial tracers, ^{14}C and ^{230}Th, suggest that particle flux along the WAP follows a long-term climatic gradient (maritime controls in the north, continental controls to the south – Smith et al., 1999), with ice-free conditions of more than 9 months a year at Sta. AA transitioning to 3 months a year ice-free at Sta. G (Smith et al., 2012). Northern stations, ice-free most of the year, receive the most particle flux, whereas the southern stations, that are ice-bound most of the year, receive the lowest particle flux (Smith et al., 1999; Smith et al., 2012).

The particle reactive tracer, ^{230}Th, is efficiently removed from the water column and indicates little net lateral transport on 1000-year timescales. On 100-year timescales, in contrast, the focusing factor derived from the ^{210}Pb data indicates that lateral transport does play an important role in scavenging particle-reactive tracers from the water column. Although the trend of decreasing particle flux with increasing latitude is maintained with the ^{210}Pb inventory data, a simple one-dimensional flux (vertical component only) cannot explain the observed inventories (Table 2).

Decadal sea-ice trends can help to explain observed particle fluxes

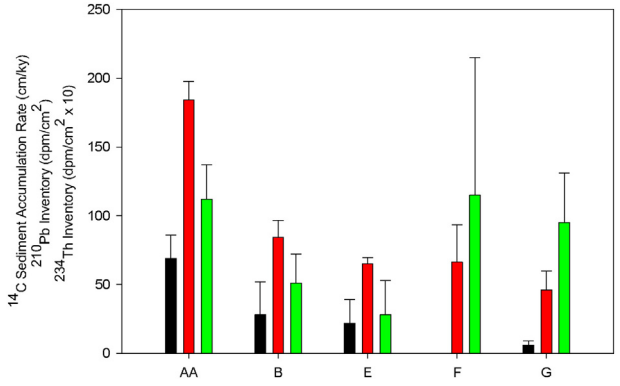

Fig. 8. Millennial (^{14}C in cm/ky - black), centurial/decadal (^{210}Pb dpm/cm^2 - red) and annual/seasonal (^{234}Th in dpm/cm^{2}x10 – green) flux proxies for the WAP. The long-term climatological trend is that of decreasing particle flux from N-S along the 550 km transect. On short time scales (seasonal to annual), there is an increase in particle flux at Stations F and G, relative to longer-term proxies, i.e., southern stations look (radiochemically) similar to the northern stations at the alpha level of 0.05. Error bars represent standard deviations of the arithmetically averaged core inventories. (For interpretation of the references to colour in this figure legend, the reader is referred to the web version of this article).

along the WAP (especially the southern stations) as open-ocean conditions increase in this area, allowing more primary production and increasing particle export from the euphotic zone, as well as facilitating resuspension and lateral transport. The high ^{234}Th seabed inventories at Stations F and G suggest that the faster rate of change in sea-ice coverage brought on by warming oceans is more important to flux dynamics in the southern, more continental stations, than at the northern, more maritime, stations (AA and B; Fig. 8).

This study used < 15% ice coverage as the criterion for ice-free days. Phytoplankton can bloom in Antarctic waters with much higher ice cover than 15%. Thus, a fruitful line of research might be to explore correlations between higher percentage ice cover days with the short-lived radioisotope inventories to explore the relationship between sea-cover and particle export to the seabed.

The long-term trends in particle flux (i.e., centurial, ^{210}Pb, and millennial, ^{14}C, timescales) both show a statistical decrease in magnitude with increasing latitude (i.e., from Sta. AA to Sta. G; Figure 8). In contrast, the seasonal and annual particle fluxes, as revealed by the ^{234}Th data, show no consistent N-S pattern or systematic relationship with sea-ice duration prior to core collection. In fact, the southern-most stations (F and G) sampled during 2008 and 2009 have statistically comparable ^{234}Th inventories to the northern-most station (Sta. AA). This pattern of particle flux on short (seasonal/annual) timescales is consistent with enhancement of particle fluxes at stations F and G in recent years, most likely induced by climate changes and decreases in sea-ice duration (Stammerjohn et al., 2008; Ducklow et al., 2013).

5. Conclusions

Over the last 50 years, higher temperatures have been recorded along the WAP; these have been correlated with sea-ice dynamics with a significant decline in sea-ice duration and an increase in open-ocean conditions, along the peninsula during the past 30 years.

Evaluation of millennial, particle flux proxies (^{230}Th- derived Psi values and ^{14}C sediment accumulation rates) reveal a N-S trend of higher particle flux at Station AA decreasing southward to Station G. Additionally, ^{210}Pb inventories display a similar gradient in particle flux along the peninsula, decreasing as latitude increases, characterizing particle flux on centurial time scales. The high ^{210}Pb inventories, relative to water column production, suggest extensive sediment focusing via lateral transport over the past 100 years. Seasonal and annual trends derived from ^{234}Th inventories along the Peninsula show an increase in particle flux at the southern stations relative to the northern stations. Although there is a discordant correlation between sea-ice days and ^{234}Th at the southern stations, data collected along the WAP suggest that the nature of particle flux has been changing in recent times, and is consistent with changes in climate and sea-ice coverage. It would appear that the decrease of sea ice, associated with warming trends on the Peninsula, is perturbing the long-term trends in particle flux, and leading to an increase in vertical transport (higher primary productivity) and lateral transport (resuspension during winter storms), especially at the southern stations, on seasonal and annual time scales.

There appears to be a systematic increase in particle flux as sea-ice diminishes, which is linked to Stations F and G exhibiting the largest and most systematic changes in sea-ice coverage over the last 35 years. The data indicate some predictive power for radioisotope inventories (^{234}Th) towards climatologically significant variables (ice coverage), but a robust model for either forecasting or reconstructing these variables has not been realized. Further investigation between ice coverage, radioisotope inventories and biogeochemical tracers, e.g., chlorophyll-a, may help to understand natural and anthropogenic forcing on particle flux along the WAP and to aid in the development of a better model for understanding climate change effects on particle flux.

Declaration of Competing Interest

The authors declare that they have no known competing financial interests or personal relationships that could have appeared to influence the work reported in this paper.

Acknowledgements

This research was part of the FOODBANCS2 Project, which was supported by the USA National Science Foundation, Polar Programs (Grant #: ANT-0636773, D. DeMaster and C.J. Thomas, PIs, and grant # ANT-0636806, C.R. Smith, PI). Brian Pointer assisted in the field collection of samples and in some of the initial radiochemical analyses. We are grateful to the captains and the crews of the R/V Nathanial B. Palmer and the R/V Laurence M. Gould for their impressive seamanship and assistance in the collection of the Antarctic samples. We are also grateful to the staff of the WHOI NOSAMS facility for their support and diligence in the measurement of the ^{14}C activities.

References

Aller, R.C., DeMaster, D.J., 1984. Estimates of particle flux and reworking at the deep-sea floor using ^{234}Th/^{238}U disequilibrium. Earth Plan. Sci. Lett. 67, 308–318.

Anadón, R., Estrada, M., 2002. The FRUELA cruises. A carbon flux study in productive areas of the Antarctic Peninsula (December 1995–February 1996). Deep-Sea Res. 49, 567–583.

Bacon, Michael P., 2004. Reactive Radionuclides as Tracers of Oceanic Particle Flux. Marine Radioactivity. Elsevier Press, Oxford, UK.

Bentley, M.J., Johnson, J.S., Hodgson, D.A., Dunia, T., Freeman, S.P.H.T., Cofaigh, C.O., 2011. Rapid deglaciation of Marguerite Bay, western Antarctic Peninsula in the early Holocene. Quat. Sci. Rev. 30, 3338–3349.

Berkman, P.A., Forman, Steven L., 1996. Pre-bomb radiocarbon and the reservoir correction for calcareous marine species in the Southern Ocean. Geophys. Res. Lett. 23 (4), 363–366.

Buessler, K.O., McDonnell, A.M.P., Schoefield, O.M.E., Steinberg, D.K., Ducklow, H.W., 2010. High particle export over the continental shelf of the West Antarctic Peninsula. Geophys. Res. Lett. 37, L22606.

Cape, M.R., Vernet, M., Kahru, M., Spreen, G., 2014. Polynya dynamics drive primary production in the Larsen a and B embayments following ice shelf collapse. J. of GeoPhys. Res. 119, 572–594.

Cape, M.R., Vernet, M., Pettit, E.C., Wellner, J.S., Truffer, M., Akie, G., Domack, E., Leventer, A., Smith, C.R., Huber, B.A., 2019. Circumpolar Deep Water impacts glacial meltwater export and coastal biogeochemical cycling along the West Antarctic Peninsula. Front. Mar. Sci. 6, 144. https://doi.org/10.3389/fmars.2019.00144.

Ducklow, H., Clarke, A., Dickhut, R., Doney, S.C., Geisz, H., Huang, K., Martinson, D.G., Meredith, M.P., Moeller, H.V., Montes-Hugo, M., Schofield, O., Stammerjohn, S.E., Steinberg, D., Fraser, W., 2012. The marine system of the Western Antarctic Peninsula. In: Antarctic Ecosystems: An Extreme Environment in a Changing World. Blackwell Publishing.

Ducklow, H.W., Fraser, W.R., Meredith, M.P., Stammerjohn, S.E., Doney, S.C., Martinson, D.G., Sailley, S.F., Schofield, O.M., Steinberg, D.K., Venables, H.J., Amsler, C.D., 2013. West Antarctic Peninsula: an ice-dependent coastal marine ecosystem in transition. Oceanography 26 (3), 190–203.
Fan, T., Deser, C., Schneider, D.P., 2014. Recent Antarctic Sea ice trends in the context of southern ocean surface climate variation since 1950. Geophys. Res. Lett. 41, 2419–2426.
Francois, R., Frank, M., Rutgers van der Loeff, M.M., Bacon, M.P., 2004. ^{230}Th normalization: an essential tool for interpreting sedimentary fluxes during the late quaternary. Paleocean. 19, PA1018.
Fritsen, C.H., Memmott, J.C., Ross, R.M., Quetin, L.B., Vernet, M., Wirthlin, E.D., 2011. The timing of sea ice formation and exposure to photosynthetically active radiation along the Western Antarctic Peninsula. Polar Biol. 34, 683–692.
García, M., Ercilla, G., Alonso, B., Casa, D., Dowdeswell, J.A., 2011. Sediment lithofacies, processes and sedimentary models in the Central Bransfield Basin, Antarctic Peninsula, since the last Glacial Maximum. Mar. Geol. 290, 1–16.
Gilbert, R., Chong, A., Dunbar, R.B., Domack, E.W., 2003. Sediment trap records of glaciomarine sedimentation at Muller ice shelf, Lallemand fjord, Antarctic Peninsula. Arctic Antarctic Alpine Res. II. 35 (1), 24–33.
Harangozo, S.A., 2006. Atmospheric circulation impacts on winter maximum sea ice extent in the West Antarctic Peninsula region (1979-2001). Geophys. Res. Lett. 33, L02502.
Harden, S.L., DeMaster, D.J., Nittrouer, C.A., 1992. Developing sediment geochronologies for high-latitude continental shelf deposits: a radiochemical approach. Mar. Geo. 103, 69–97.
Heroy, D.C., Anderson, J.B., 2007. Radiocarbon constraints on Antarctic Peninsula Ice Sheet retreat following the last Glacial Maximum (LGM). Quat. Sci. Rev. 26, 3286–3297.
Hillenbrand, C.-D., Grobe, H., Diekmann, B., Kuhn, G., Futterer, D.K., 2003. Distribution of clay minerals and proxies for productivity in surface sediments of the Bellingshausen and Amundsen seas (West Antarctica) – relation to modern environmental conditions. Mar. Geol. 193, 253–271.
Hillenbrand, C.D., Camerlenghi, A., Cowan, E.A., Hernandez-Molina, F.J., Lucchi, R.G., Rebesco, M., Uenzelmann-Neben, G., 2008. The present and past bottom-current flow regime around the sediment drifts on the continental rise west of the Antarctic Peninsula. Mar. Geol. 255, 55–63.
Isla, E., Masqué, P., Palanques, A., Guillen, J., Puig, P., Sanchez-Cabeza, J.A., 2004. Sedimentation of biogenic constituents during the last century in western Bransfield and Gerlache Straits, Antarctica: a relation to currents, primary production, and sea floor relief. Mar. Geol. 209, 265–277.
Jacobs, S.S., Comiso, J.C., 1993. A recent sea-ice retreat west of the Antarctic Peninsula. Geophys. Res. Lett. 20, 1171–1174.
Khim, B.K., Shim, J., Yoon, H.I., Kang, Y.C., Jang, Y.H., 2007. Lithogenic and biogenic particle deposition in an Antarctic coastal environment (Marian Cove, King George Island): seasonal patterns from a sediment trap study. Estuarin Coastal Shelf Sci. 73, 111–122.
Ku, T., Lin, M., 1976. ^{226}Ra distributions in the Antarctic Ocean. Earth Plan. Sci. Lett. 32, 236–248.
Masqué, P., Isla, E., Sanchez-Cabeza, J.A., Palanques, A., Bruach, J.M., Guillen, J., 2002. Sediment accumulation rates and carbon fluxes to bottom sediments at the Western Bransfield Strait (Antarctica). Deep-Sea Res. II 49, 921–933.
Mayewksi, P.A., Meredith, M.P., Summerhayes, C.P., Turner, J., Worby, A., Barrett, P.J., Casassa, G., Bertler, N.A.N., Bracegirdle, T., Naveira Garabato, A.C., Bromwich, D., Campbell, H., Hamilton, G.S., Lyons, W.B., Maasch, K.A., Aoki, S., Xiao, C., van Ommen, T., 2009. State of the Antarctic and southern ocean climate system. Rev. Geophys. 47, RG1003.
McClintic, M.A., DeMaster, D.J., Thomas, C.J., Smith, C.R., 2008. Testing the FOODBANCS hypothesis: seasonal variations in near-bottom particle flux, bioturbation intensity, and deposit feeding based on ^{234}Th measurements. Deep-Sea Res. 55, 2425–2437.
McClintock, J., Ducklow, H., Fraser, W., 2008. Ecological responses to climate change on the Antarctic Peninsula. Amer. Sci. 96, 302–310.
McGinnis, J.P., Hayes, D.E., Driscoll, N.W., 1997. Sedimentary processes across the continental rise of the southern Antarctic Peninsula. Mar. Geol. 141, 91–109.
Meredith, M.P., King, J.C., 2005. Rapid climate change in the ocean west of the Antarctic Peninsula during the second half of the 20th Century. Geophys. Res. Lett. 32, L19604.
Mincks, S.L., Smith, C.R., DeMaster, D.J., 2005. Persistence of labile organic matter and microbial biomass in Antarctic shelf sediments: evidence of a sediment "food bank". Mar. Ecol. Prog. Ser. 300, 3–19.
Moffat, C., Beardsley, R.C., Owens, B., van Lipzig, N., 2008. A first description of the Antarctic Peninsula coastal current. Deep-Sea Res. 55, 277–293.
Montes-Hugo, M., Doney, S.C., Ducklow, H.W., Fraser, W., Martinson, D., Stammerjohn, S.E., Schofield, O., 2009. Recent changes in phytoplankton communities associated with rapid regional climate change along the Western Antarctic Peninsula. Sci. 323, 1470–1473.
Mulvaney, R., Abram, N.J., Hindmarsh, R.C.A., Arrowsmith, C., Fleet, L., Triest, J., Sime, L.C., Alemany, O., Foord, S., 2012. Recent Antarctic Peninsula warming relative to Holocene climate and ice-shelf history. Nature 489, 141–145.
Palanques, A., Isla, E., Masqué, P., Puig, P., Sanchez-Cabeza, J.-A., Gili, J.M., Guillen, J., 2002. Downward particle fluxes and sediment accumulation rates in the western Bransfield Strait: implications of lateral transport for carbon cycle studies. J. Mar. Res. 60, 347–365.
Pilson, Michael E.Q., 2012. An Introduction to the Chemistry of the Sea. Pearson Education. Prentice-Hall, NJ, USA.
Pirtle-Levy, Rebecca S., 2016. Lipid-Based Investigation of Food-Web Dynamics for the Benthic Community of the West Antarctic Peninsula. Doctoral Dissertation. North Carolina State University, pp. 145.
Purinton, B.L., DeMaster, D.J., Thomas, C.J., Smith, C.R., 2008. ^{14}C as a tracer of labile organic matter in Antarctic benthic food webs. Deep-Sea Research II. 55, 2438–2450.
Rozema, P.D., Vernables, H.J., van de Poll, W.H., Clarke, A., Meredith, M.P., Buma, G.J., 2016. Interannual variability in phytoplankton biomass and species composition in northern Marguerite Bay (West Antarctic Peninsula) is governed by both winter sea ice cover and summer stratification. Limnol. Oceanog. 62, 235–252.
Savidge, D.K., Amft, J.A., 2009. Circulation on the West Antarctic Peninsula derived from 6 years of shipboard ADCP transects. Deep-Sea Res. 56, 1633–1655.
Smith, W.O., Nelson, D.M., 1985. Phytoplankton bloom produced by a receding ice edge in the Ross Sea: spatial coherence with the density field. Science. 227 (4683), 163–166.
Smith, R.C., Ainley, D., Baker, K., Domack, E., Emslie, S., Fraser, B., Kennett, J., Leventer, A., Mosley-Thompson, E., Stammerjohn, S., Vernet, M., 1999. Marine ecosystem sensitivity to climate change. BioScience. 49 (5), 393–404.
Smith, R.C., Martinson, D.G., Stammerjohn, S.E., Iannuzzi, R.A., Ireson, K., 2008a. Bellingshausen and Western Antarctic Peninsula region: pigment biomass and sea-ice spatial/temporal distributions and interannual variability. Deep-Sea Res. II 55, 1949–1963.
Smith, C.R., Mincks, S., DeMaster, D.J., 2008b. The FOODBANCS project: introduction and sinking fluxes of organic carbon, chlorophyll-a and phytodetritus on the western Antarctic Peninsula continental shelf. Deep-Sea Res. II 55, 2404–2414.
Smith, C.R., DeMaster, D.J., Thomas, C., Srsen, P., Grange, L., Evrard, V., DeLeo, F., 2012. Pelagic-benthic coupling, food banks, and climate change on the West Antarctic Peninsula shelf. Oceanography. 25 (3), 188–201.
Stammerjohn, S.E., Martinson, D.G., Smith, R.C., Iannuzzi, R.A., 2008. Sea ice in the Western Antarctic Peninsula region: spatio-temporal variability from ecological and climate change perspectives. Deep-Sea Res. 55, 2041–2058.
Taylor, F., Whitehead, J., Domack, E., 2001. Holocene paleoclimate change in the Antarctic Peninsula: evidence from the diatom, sedimentary and geochemical record. Mar. Micropaleo. 41, 25–43.
Turner, J., Maksym, T., Phillips, T., Marshall, G.J., Meredith, M.P., 2013. The impact of changes in sea ice advance on the large winter warming on the western Antarctic Peninsula. Int. J. Climatol. 33, 852–861.
Turner, J., Barrand, N.E., Bracegirdle, T.J., Convey, P., Hodgson, D.A., Jarvis, M., Jenkins, A., Marshall, G., Meredith, M.P., Roscoe, H., Snaklin, J., 2014. Antarctic climate change and the environment: an update. Polar Rec. 50, 237–259.
Turner, J., Lu, H., White, I., et al., 2016. Absence of 21st century warming on Antarctic Peninsula consistent with natural variability. Nature 535, 411–415. https://doi.org/10.1038/nature18645.
Weston, K., Jickells, T.D., Carson, D.S., Clarke, A., Meredith, M.P., Brandon, M.A., Wallace, M.I., Ussher, S.J., Hendry, K.R., 2013. Primary production export flux in Marguerite Bay (Antarctic Peninsula): linking upper water-column production to sediment trap flux. Deep-Sea Res. I 75, 52–66.